Effect of Mixed Fullerene Ratio on the Optical and Electrical Properties of P3HT: ICxA Bulk Heterojunction Thin Films and Optical Modelling of OPV Devices.

Noor Al-Huda H. Ali and Mohammed F. Al-Mudhaffer*

Department of Physics, College of Education for Pure Sciences, Basrah, Iraq.

***Corresponding author E-mail:** mohammed.al-mudhaffer@uobasrah.edu.iq

https://doi.org/10.29072/basjs.20260118

ARTICLE INFO

Received: 19 October 2025

Accepted: 12 January 2026

Published: 30 April 2026

Keywords:

ICxA, Optical properties, Electrical properties, Thermal effect on OPVs.

ABSTRACT

A series of P3HT: ICxA BHJ thin films was prepared with different donor–acceptor ratios to assess the influence of fullerene concentration on the optical and electrical properties of the active layer. Six acceptor ratios were considered (1:0.5, 1:0.8, 1:1, 1:1.2, 1:1.5 and 1:2) in this article. The topography of the surface was examined by capturing the AFM images, which confirmed that all samples exhibited an RMS of roughness (2~4 nm). The optical measurements of P3HT: ICxA revealed that the blending ratio (1:1.2) exhibited the highest optical response in comparison with other samples. For all films, the absorption coefficient satisfied $\alpha > 10^4$ cm^{-1}, indicating the occurrence of direct electronic transitions within the active layer. Electrical measurements as a function of sample temperature were demonstrated in the range of (25- 65 ºC) at dark and light conditions. A photoactive layer, P3HT: ICxA, generates relatively similar values of current in both heating and cooling cycles, that suggested active layer morphology optimized and remained well-ordered throughout the thermal process. Finally, optical modelling of a complete OPV device was performed, and its results supported and confirmed the trends observed in both the optical and electrical measurements.

1. Introduction

Bulk heterojunction organic photovoltaics (BHJ-OPVs) have received more attention from researchers due to their advantages, such as ease of processing, versatility, cost-effectiveness,

low-light performance, and ability to harvest energy across the entire solar spectrum [1, 2]. The fabrication and efficiency of OPVs have seen significant improvements in the past two decades. For instance, the performance record exceeds 19% for small-scale single junction devices[3, 4], compared with 12% for large-scale OPV (4100 cm^2) [5, 6]. As such, the OPVs' improvements involved indoor applications due to their ability to work effectively under low-light and artificial lighting conditions[7, 8]. Nowadays, in organic photovoltaics, various architectures have been created over time, such as single-layer, bilayer, bulk heterojunction, and tandem OPV cells. Each type of photoactive morphology has distinct advantages and disadvantages [9]. In general, the photoactive layer of bulk heterojunction devices is comprised of a blend of electron donor and acceptor material can function correctly based on the energy level alignments with sufficient offset between the highest occupied molecular orbital (HOMO) and lowest unoccupied molecular orbital (LUMO) to achieve a high rate of exciton dissociation [10]. When OPV devices are illuminated by sunlight, the exciton, which is a pair of electron/holes at critical conditions, will be generated in the electron-donating material. Subsequently, the exciton dissociated at the donor/acceptor interface to a free electron and a hole. The free electron will transport through the electron-accepting material until the collection point at the cathode, whereas a free hole will move on the opposite side to accumulate at the anode layer, respectively [9]. A common donor material in the photoactive layer in OPVs is a poly (3-hexylthiophene) (P3HT) with an energy gap of ~1.93 eV, blended with an acceptor material, 1-(3-methoxycarbonyl) propyl-1-phenyl [6,6]C61 (PCBM) represented the most extensively researched active materials of the bulk-heterojunction OPVs [11]. However, ICxA acceptor in 2016 was introduced as a cost-effective acceptor substitute for PCBM or ICBA in both small-scale and roll-to-roll printed devices, with comparable power conversion efficiency. This acceptor is expected to facilitate the commercialization of organic photovoltaics (OPV) and substantially reduce the cost barrier for research organizations aiming to transfer to roll-to-roll printing[12]. To optimize the charge generation process in the donor/acceptor blend of BHJ-OPVs, with achieving an electron diffusion length of ~10 nm, as is well known in the literature, the active layer morphology must be engineered to be in similar electron diffusion length [10]. Therefore, the molecular engineering of materials, the donor-to-acceptor ratio, varying D–A device construction ratios, and diverse fabrication procedures (such as thermal annealing, solvent selection, and solvent additive processing) can optimize the efficiency of BHJ OSCs[13].

In this report, the active layer was prepared from (P3HT: ICxA) for BHJ-OPVs based on altering the acceptor ratio, in order to determine the acceptor effect on optical and electrical properties of the active layer. Surface morphology of the active layer was determined by taking AFM images, followed by UV-vis measurements to identify the optical properties of the samples. Electrical measurements (including recorded current, conductivity, and resistivity) were conducted at room temperature and at light and dark conditions using an LED light source with an illuminated power of 50 mW/cm^2. Then the electrical measurements were implemented as a function of altering the temperature in the range (25 ~65 °C) during heating and cooling cycles in dark and under light conditions. This work systematically links surface morphology, optical properties, and electrical behavior to changes in acceptor concentration. In addition, temperature-dependent electrical measurements were carried out under both dark and illuminated conditions during heating and cooling cycles, providing insight into the thermal stability and charge transport behavior of the active layer. Finally, experimental results were supported by conducting the optical modelling to predict full OPV device performance, offering a more complete understanding of the structure–property–performance relationship in P3HT: ICxA systems.

2. Materials and Methods

2.1 Materials

A photoactive materials Poly(3-hexylthiophene) (P3HT) (MW 40 kD) and ICxA (a low cost fullerene mixture of mono-, bis-, and tris- adducted indene C60 consisting of 53% indene-C60 bisadduct (ICBA), 36% indene-C60 monoadduct (ICMA), and 11% indene-C60-tris-adduct (ICTA)) were provided from the centre for Organic electronics-University of Newcastle -Au where they were synthesized and published previously [16]. The chloroform was purchased from Central Drug House LTD. The interdigitated Indium tin oxide (ITO) substrates (with a channel length of 50 μm) were purchased from Ossila Company, UK.

2.2 Sample preparation

A combination of ratios of donor and acceptor materials was inserted in Table 1. To prepare the BHJ photoactive layer solution, 1 mL of chloroform solvent was added to each sample, then sonicated for 45 min in a water bath Sonicator (has power 40 mW). Then, 6 samples of the active layer were spun on an interdigitated substrate using a 2000 rpm spin speed. Finally, the samples were annealed, using a hot plate at 140 °C for 4 min. All the active layer preparation steps are illustrated in Figure 1.

Table 1. The blending ratios of P3HT: ICxA to prepare the photoactive layer solution.

Sample Id:	(P3HT: ICxA)	P3HT(mg)	ICxA(mg)
S1	(1:0.5)	10	5
S2	(1:0.8)	10	8
S3	(1:1)	10	10
S4	(1:1.2)	10	12
S5	(1:1.5)	10	15
S6	(1:2)	10	20

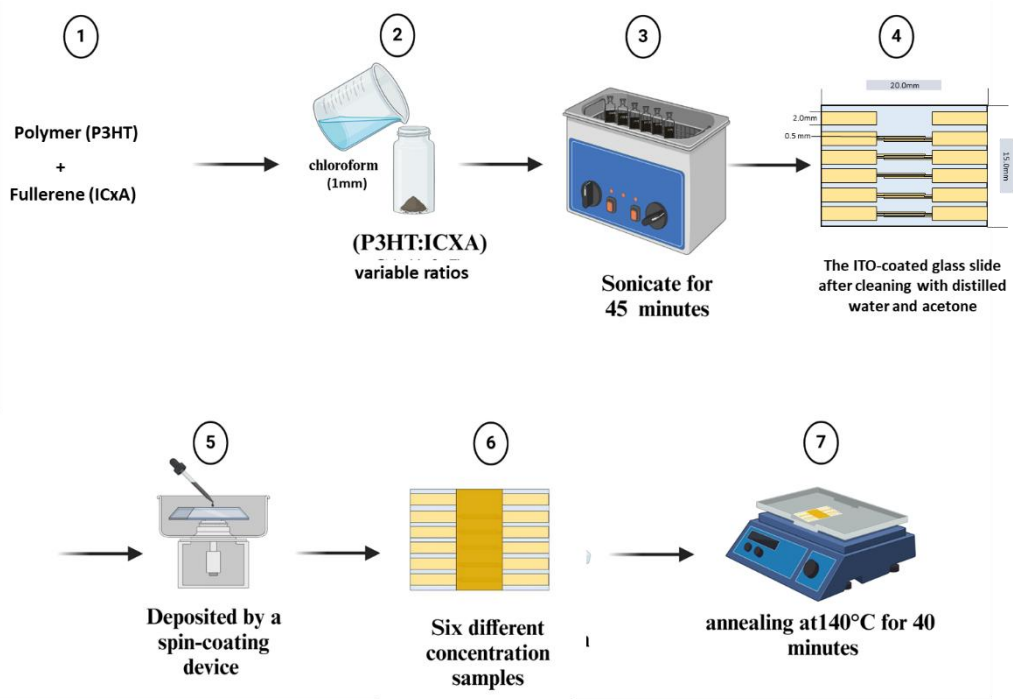

Figure 1. Presents the active layer thin films preparation steps using varied acceptor ratios as follows: (S1 (P3HT: ICxA (1:0.5)), S2 (P3HT: ICxA (1:0.8)), S3 (P3HT: ICxA (1:1)), S4 (P3HT: ICxA (1:1.2)), S5 (P3HT: ICxA (1:1.5)), and S6 (P3HT: ICxA (1:2)) dissolved in Chloroform.

2.3 Surface Characterization

To investigate the surface morphology of P3HT: ICxA with a varied ratio, the atomic force microscopy (AFM) measurements were conducted. For all samples, the active layer solution was spun on glass substrates, then annealed at 140 °C for 4 min, and the AFM images are illustrated in Figure 2.

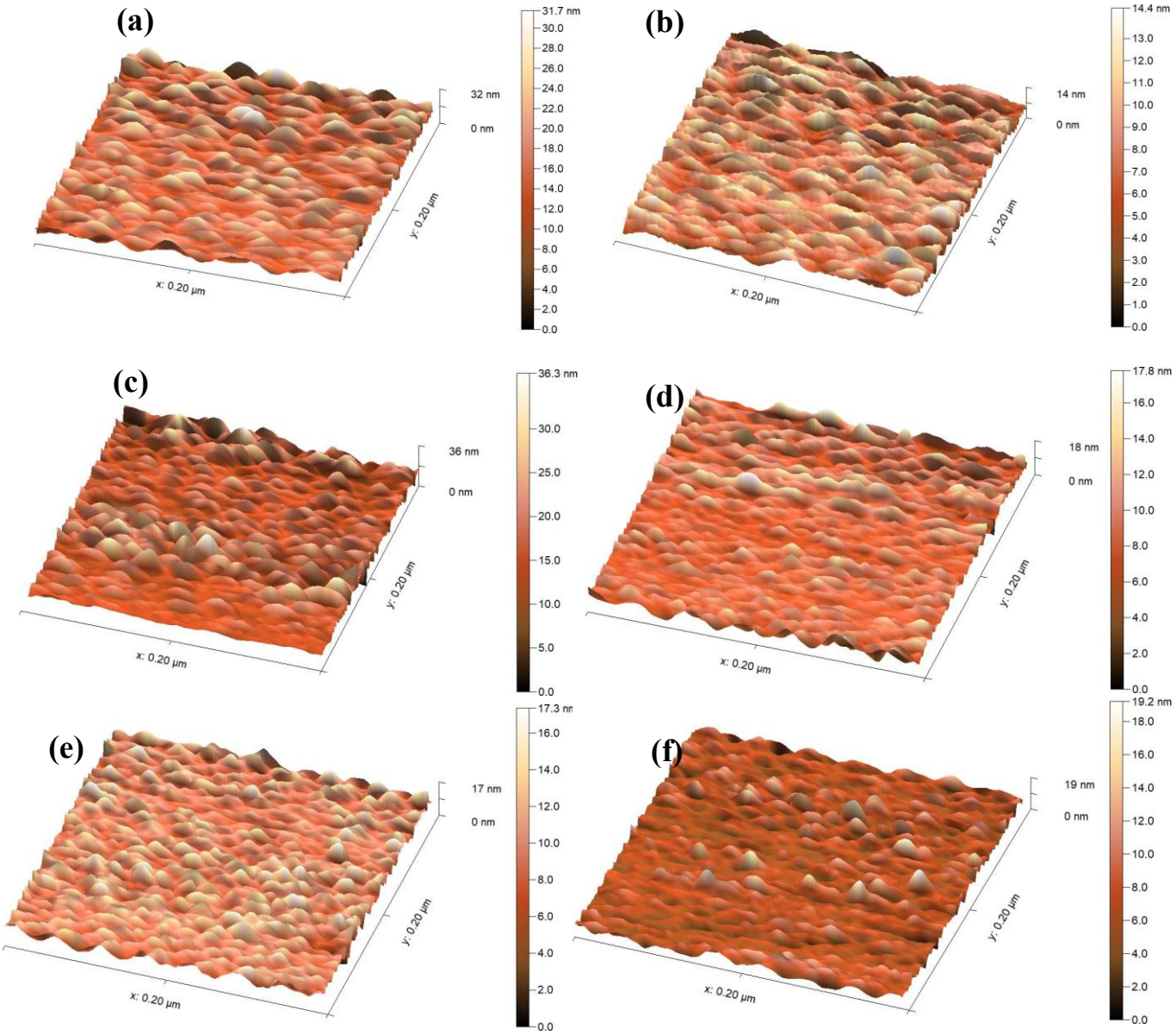

Figure 2. Presents the AFM images of P3HT: ICxA varied fullerene ratio as follows: ((a) (1:0.5), (b) (1:0.8), (c) (1:1), (d) (1:1.2), (e) (1:1.5), and (f) (1:2)) annealed at 140 °C for 4 minutes.

The surface morphology images of all samples revealed that the nature of the surface is homogeneous at the microscale, and no clear phase separation for ICxA was observed. As presented in Table 2, the surface RMS roughness varied from 4 nm to 2 nm for samples (S1-S6) and a peak-to-valley distance of <23.78 nm. These RMS roughness values within the range of a common P3HT: ICBA that was reported previously to be 0.1~10 nm [14].

Table 2. The surface roughness values of P3HT: ICxA ratios material to prepare the photoactive layer solution.

Sample ID:	Average value(nm)	RMS roughness (Sq)(nm)	Mean roughness (nm)
S1 (P3HT: ICxA (1:0.5))	23.7879	4.11695	3.15108
S2 (P3HT:ICxA (1:0.8))	7.601	2.18712	1.75462
S3 (P3HT:ICxA (1:1))	18.7981	3.99522	2.86354
S4 (P3HT:ICxA (1:1.2))	19.8985	2.90854	2.15372
S5 (P3HT:ICxA (1:1.5))	10.302	2.00537	1.52949
S6 (P3HT:ICxA (1:2))	8.0342	2.00217	1.5364

2.4 Optical Simulation

In this report, the optical modelling was applied to predict the internal light absorption (the active layer performance) in the organic photovoltaics devices or a multilayer system. This theoretical treatment relies on the actual UV-vis measurements of the active layer thin film. Then, two software were employed to conduct the optical simulation: Reffit and MATLAB[15] [16]. The initial step was identifying the complex dielectric function (DE) from fitting the UV-vis measurements (i.e., reflection and transmission data of all samples) with the theoretical oscillator models using Reffit software [18]. In MATLAB code, the incident light diffuses in one dimension in a multi-layer system, considering that all device layers are parallel and flat interfaces, isotropic and homogeneous [17]. The internal light absorption of the active layer will be calculated by finding the negative derivative of the Poynting vector using the following relation, that programming in MATLAB [18] :

$$Q(x) = \frac{1}{2}\,\omega_o \varepsilon_o \varepsilon_2\,|E(x)|^2 \qquad \textbf{Eq.1}$$

Where $\varepsilon_o \varepsilon_2$ are the vacuum permittivity and imaginary part of the dielectric function.

3. Results and discussion

Due to the application of P3HT: ICxA material in OPV devices, it is an important step to identify its optical properties by performing the UV-vis measurements for all samples (S1 to S6) in the wavelength range (300-800 nm). All the optical measurements, for instance, reflectance and transmittance (RT), were presented in Figure 3. There are two discrete regimes in RT spectra, in (300-400 nm) referred to as the fullerene absorption (ICxA), and 400-650 nm is the polymer material (P3HT) absorption [19].

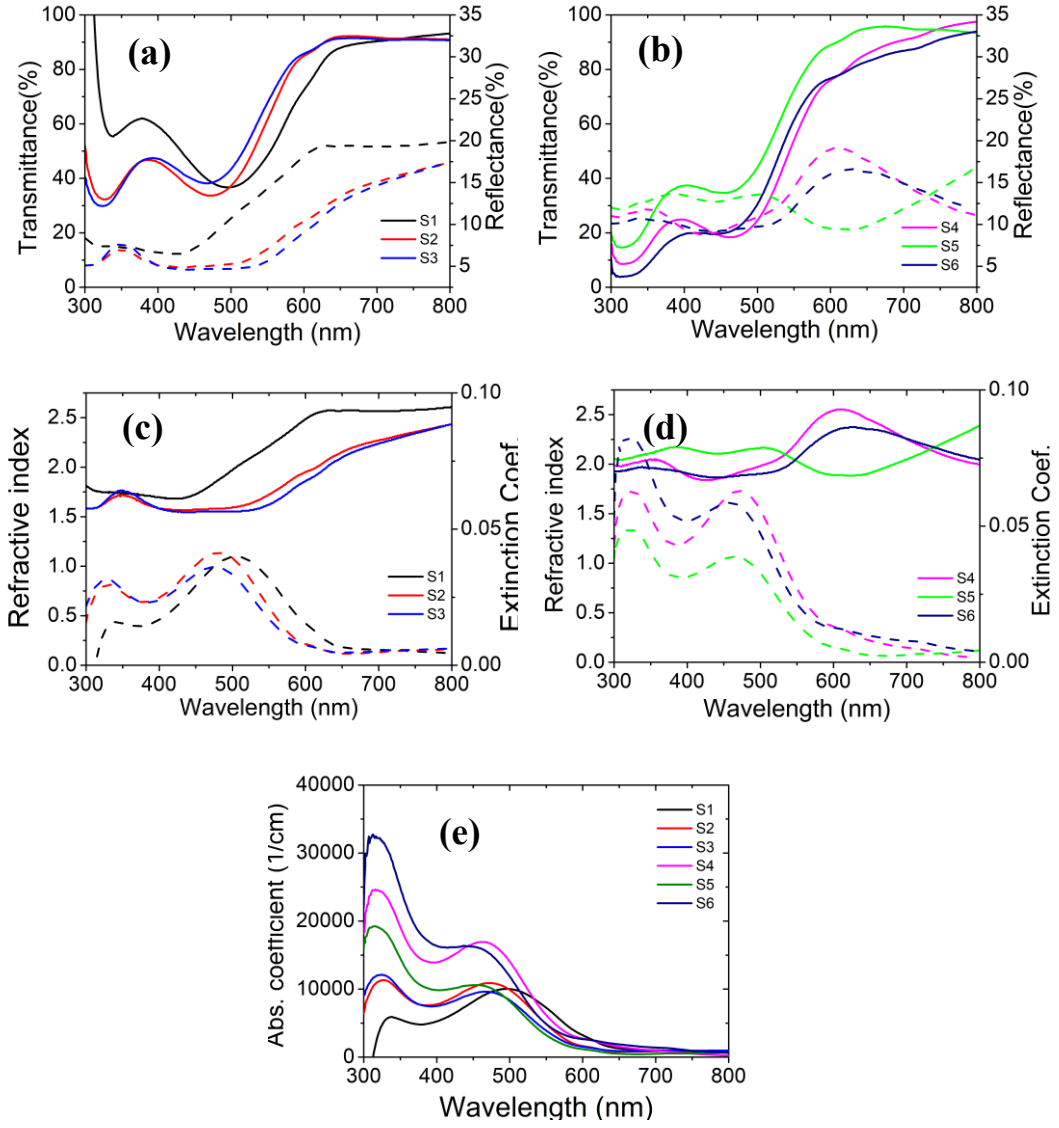

Figure 3. (a and b) presented the transmittance and reflectance spectra for (S1 (P3HT: ICxA (1:0.5)), S2(P3HT: ICxA (1:0.8)), S3(P3HT: ICxA (1:1)), S4 (P3HT: ICxA (1:1.2)), S5 (P3HT: ICxA (1:1.5)) and S6 (P3HT: ICxA (1:2))), (c and d) shown reflective index and extinction coefficient and (e) is the absorption coefficient of all samples.

The effect of increasing the fullerene material (ICxA) percentage was clear in the absorption and excitation coefficient in the wavelength range (300-400 nm), whereas the polymer (P3HT) absorption regime (400-650 nm) remained without a noticeable enhancement. Figures 3c and d show the reflective index of the sample and its values ~2, whereas the excitation coefficient that describes the interaction of incident light with material (or represents the light absorption of incident light in this material) values alter (from 0.05 ~0.07). A general trend of samples is the k increased with a fullerene ratio which meant samples (S5 and S6) absorbs more light leading to create more free charge, however, this trend didn't achieved in the electrical measurement later in this report due to increasing fullerene ratio can be improved the defects in the material so the charge traps and recombination process will be increased. From the absorption coefficient values (see Figure 3 (e)), the type of electronic transition in P3HT: ICxA active layer is direct, as the values of the absorption coefficient ($\alpha > 10^4$ cm^{-1}) [20].

To address the effect of fullerene mixing ratio on the active layer performance, the electrical measurements were conducted to clarify the best blending ratio that can be used with this type of donor and acceptor materials. Electrical measurements in this report were conducted at dark, light conditions and the recorded current as a function of varying temperature conditions (25-65 °C) using a light source LED with an intensity of 50 mW/cm^2. All *I–V* characterization of samples was executed using the Keithley 236 source measurement unit. In dark conditions, the applied voltage was varied from 0.5 to 10 V, and the recorded current, conductivity, and resistivity are shown in Figure 4. Sample S4 exhibited the highest values of current (I_{max} =4.2 µA at V_{app}=10 V) in comparison with 57%, 69%, 51% , 75% , 59% then (S1,S2,S3,S5 and S6) respectively .

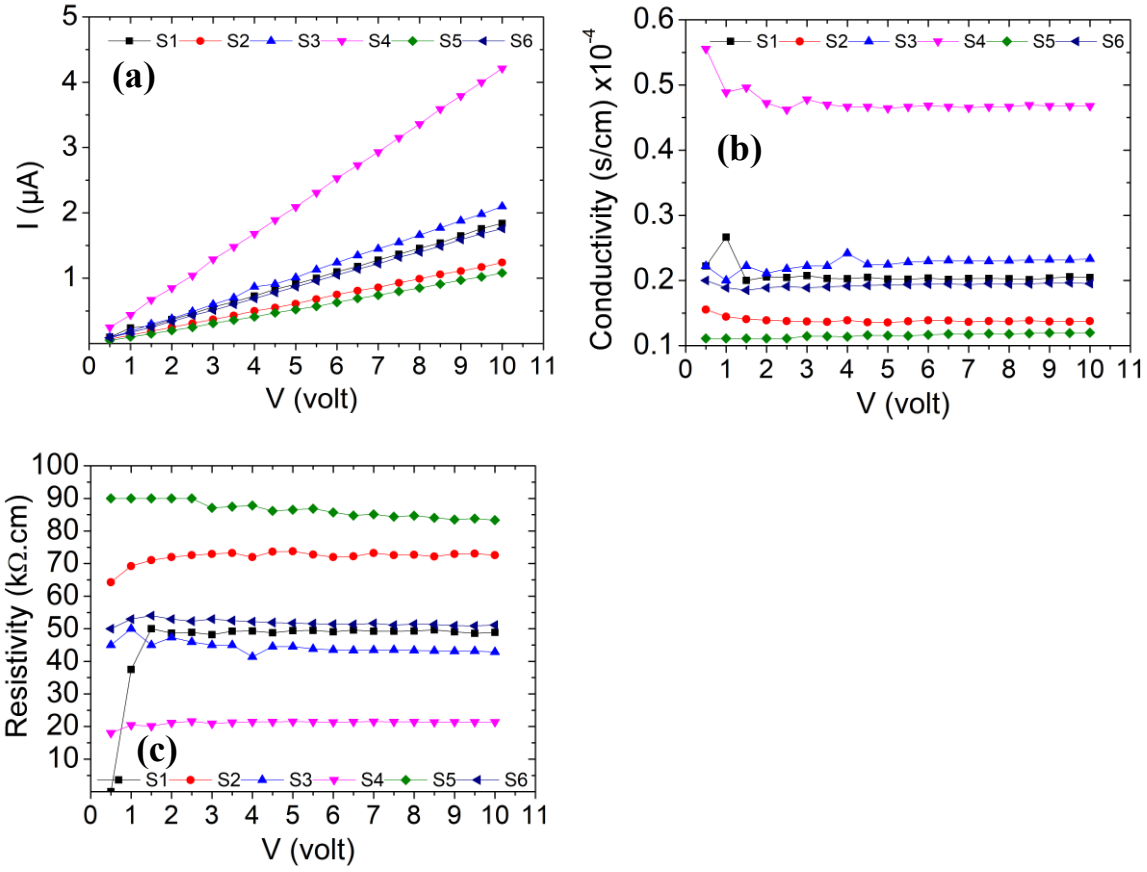

Figure 4. Presents the electrical measurements (a) the recorded current (b) conductivity and (c) is the resistivity at dark conditions for samples series (S1 (P3HT: ICxA (1:0.5)), S2(P3HT: ICxA (1:0.8)), S3(P3HT: ICxA (1:1)), S4 (P3HT: ICxA (1:1.2)), S5 (P3HT: ICxA (1:1.5)) and S6 (P3HT: ICxA (1:2))).

A similar behavior was noticed in conductivity and resistivity values, where the conductivity value of S4 is 0.46778×10^{-4} S/cm associated with a lower resistivity value of about ~20 kΩ.cm whereas the resistivity of other samples altered in the range (42 – 83 kΩ.cm), and the behavior is a saturated trend for both conductivity and resistivity with increasing the applied voltage. In

Figure 5, the electrical measurements of all samples (S1 to S6) under light conditions are illustrated. In this case, there are two main source lead to the generation of free charge carriers, which are the applied voltage and the absorption of incident light, creating pairs of electron /hole at a critical concentration, and they can be dissociated at the donor /acceptor interface [21]. These measurements revealed another time that sample S4 with a mixing ratio of P3HT:

ICxA (1:1.2) exhibited the optimum performance. It generated current (5.25 µA), which increased by 2.178, 3.241, 1.895, 3.889, and 2.983 times compared with other samples (See Table 3).

Table 3. Electrical measurements recorded current, conductivity, and resistivity for P3HT: ICxA varied acceptor ratio at room temperature using an LED as a light source (50mW/cm^2) and at an applied voltage of 10 V.

Sample ID:	I (µA)	σ (S/cm) x10^{-4}	r (kΩ.cm)	Enhancement (times) compared with S4
S1	2.41	0.268	37.344	2.178
S2	1.62	0.180	55.556	3.241
S3	2.77	0.308	32.491	1.895
S4	5.25	0.583	17.143	1.000
S5	1.35	0.150	66.667	3.889
S6	1.76	0.196	51.136	2.983

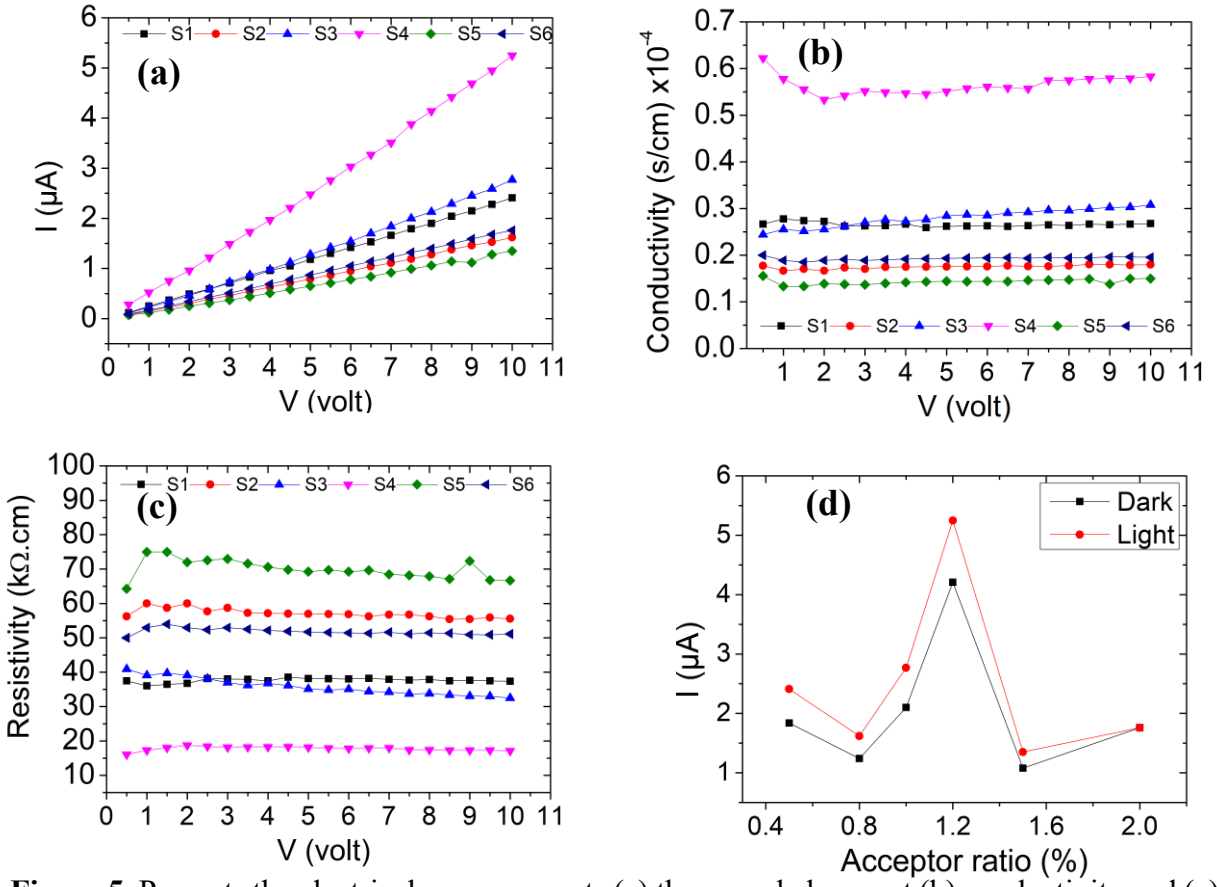

Figure 5. Presents the electrical measurements (a) the recorded current (b) conductivity and (c) is the resistivity at light conditions for samples series (S1 (P3HT: ICxA (1:0.5)), S2(P3HT: ICxA (1:0.8)), S3(P3HT: ICxA (1:1)), S4 (P3HT: ICxA (1:1.2)), S5 (P3HT: ICxA (1:1.5)) and S6 (P3HT: ICxA (1:2))). , finally , (d) shows the acceptor ratio effect on the recorded current.

According to previous reports, the best donor /acceptor mixing ratio is (1:0.8) and (1:1); however, in this study, the active layer was spun on an interdigital substrate, which means the active layer performance seems slightly altered from the sandwich devices in solar cells. To continue the optimization process of all samples, the electrical measurements of all samples (S1 to S6) were conducted. Two cycles were performed in these measurements, a heating cycle as the temperature increased from 25 to 65 °C, followed immediately by a cooling cycle, with the generated current in both cases at dark and light conditions. The recorded current, conductivity, and resistivity of all samples were presented in Figure 6 at dark conditions using an applied voltage of 10 V.

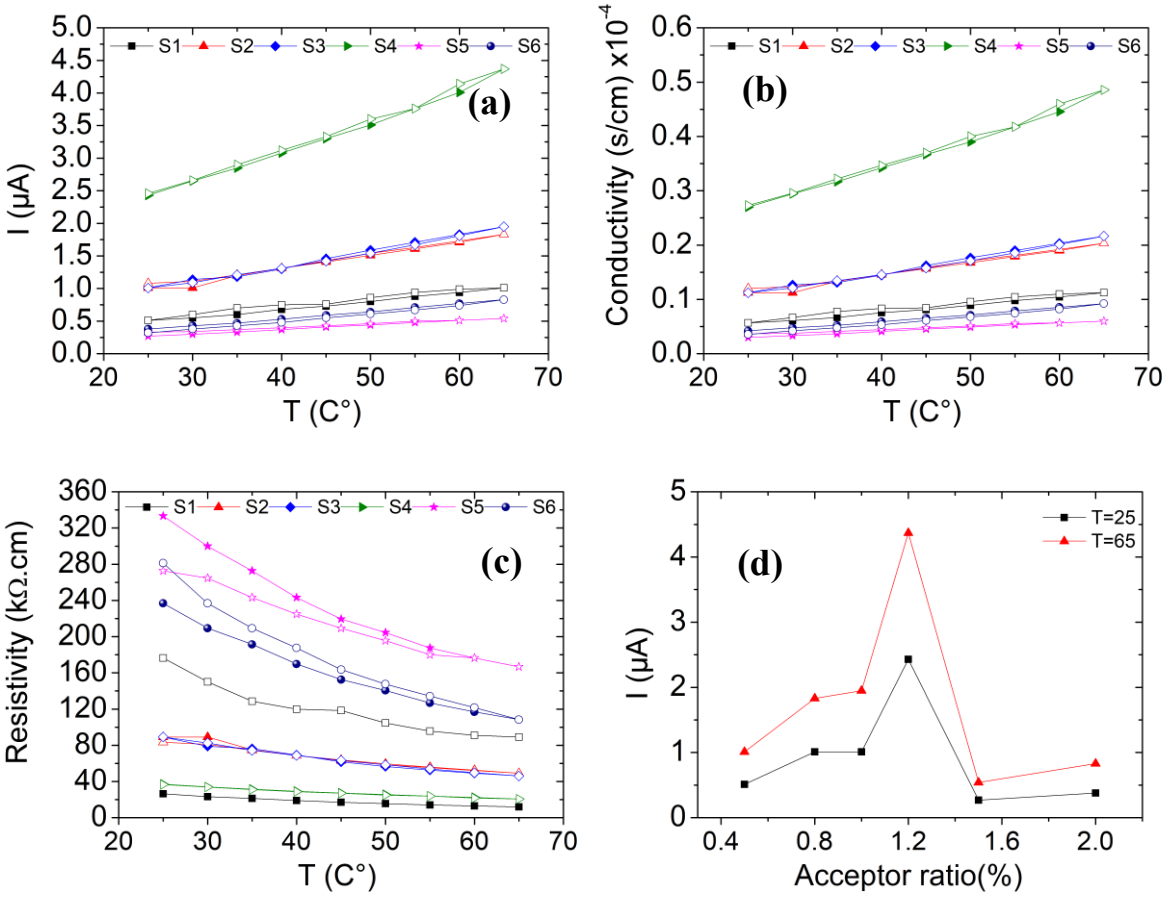

Figure 6. presents the electrical measurements (a) the recorded current (b) conductivity and (c) is the resistivity at dark conditions for samples series (S1 (P3HT: ICxA (1:0.5)), S2(P3HT: ICxA (1:0.8)), S3(P3HT: ICxA (1:1)), S4 (P3HT: ICxA (1:1.2)), S5 (P3HT: ICxA (1:1.5)) and S6 (P3HT: ICxA (1:2)))as function of temperature of (25-65 °C) using 10 V applied voltage. (d) Shows the temperature effect on the recorded current at a varied acceptor ratio.

The findings of this part confirmed the previous results of this report as S4 with mixing ratio (1:1.2) exhibited a highest recorded current (4.37 μA) in comparison to (0.51, 1.01, 0.27 and 0.38 μA) of samples (S1, S2, S3, S5 and S6) respectively, associated with increasing percentage (79, 58, 55, 58, 88 and 84%) compared with S1, S2, S3, S5 and S6 respectively at both 25 and 65 ºC. In addition, the heating and cooling cycle measurements are relatively close in the recorded values, which confirms the morphology of the active layer was well oriented and improved with increasing the temperature.

The morphology improvement was preserved in the cooling cycle as the recorded current values remain approximately in range with the heating cycle (see

Figure 5 a). Likewise, the conductivity exhibited a similar behavior to the current, which increased with temperature as its values are inserted in **Error! Not a valid bookmark self-reference.**. In

Figure 5 d, the difference between the recorded current at 25 and 65 ºC for all samples and the enhancement in the current is identified to be 1 to 2 times.

Table 4. Electrical measurements recorded current, conductivity, and resistivity for P3HT: ICxA varied acceptor ratio at temperatures of 25 and 65°C using dark conditions.

	T=25°C			T=65°C		
Sample ID:	**I (μA)**	**σ (S/cm) x10^{-4}**	**ɾ (kΩ.cm)**	**I (μA)**	**σ (S/cm) x10^{-4}**	**ɾ (kΩ.cm)**
S1	0.51	0.057	26.316	1.01	0.112	12.048
S2	1.01	0.112	89.109	1.83	0.203	49.180

S3	1.01	0.112	89.109	1.95	0.217	46.154
S4	2.43	0.270	37.037	4.37	0.486	20.595
S5	0.27	0.030	333.333	0.54	0.060	166.667
S6	0.38	0.042	236.842	0.83	0.092	108.434

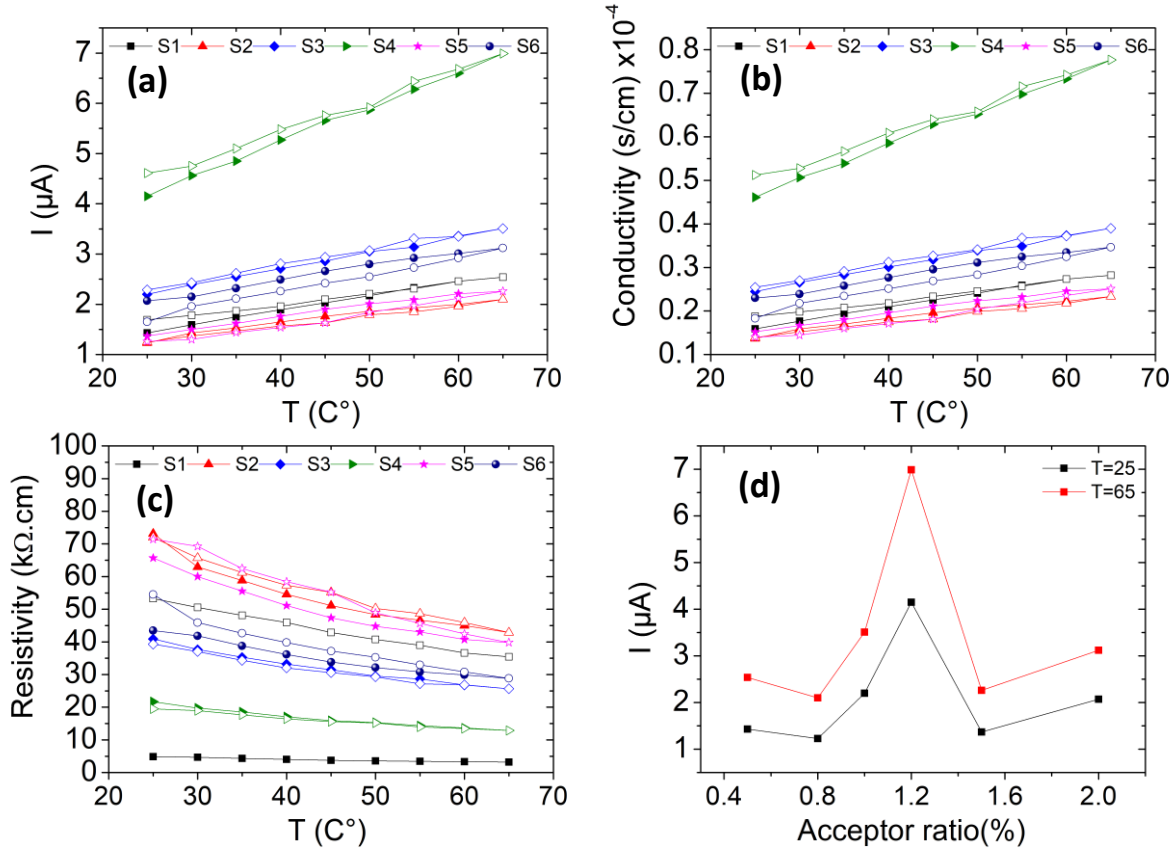

Figure 7. Presents the electrical measurements (a) the recorded current (b) conductivity and (c) is the resistivity at light conditions for samples series (S1 (P3HT: ICxA (1:0.5)), S2(P3HT: ICxA (1:0.8)), S3(P3HT: ICxA (1:1)), S4 (P3HT: ICxA (1:1.2)), S5 (P3HT: ICxA (1:1.5)) and S6 (P3HT: ICxA (1:2)))as function of temperature of (25~65 °C) using 10 V applied voltage.

.(d) shows the temperature effect on the recorded current at a varied acceptor ratio at light conditions. (d) Shows the temperature effect on the recorded current at a varied acceptor ratio.

The thermal effect on the electrical measurements of all samples was examined at light conditions using an LED light source 50 mW/cm^{2,} as shown in Figure 7. Initially, under light conditions, the electric measurements (current and conductivity) were enhanced by 2 times compared with dark conditions. All the electrical parameters for dark presented in the tables, illustrating the electrical properties at light conditions. These improvements can be referred to as increasing the internal charge generation process in the photoactive layer (P3HT: ICxA), as the thermal effect aids in creating free charges by enhancing activated hopping and improved polymer chain dynamics that enhance the free charge transport[22]. Also, it leads to rise the P3HT crystallinity and optimized phase separation, creating efficient charge transport pathways. Additionally, higher temperatures reduce recombination losses by releasing trapped charge carriers and accelerating their movement. Exciton dissociation is also facilitated, improving charge generation efficiency[23].

Table 5. Electrical measurements recorded current, conductivity, and resistivity for P3HT: ICxA varied acceptor ratio at temperatures of 25 and 65°C using an LED as a light source (50mW/cm^2).

Sample ID:	T=25°C I (µA)	T=25°C σ (S/cm) x10^{-4}	T=25°C ρ (kΩ.cm)	T=65°C I (µA)	T=65°C σ (S/cm) x10^{-4}	T=65°C ρ (kΩ.cm)
S1	1.430	0.159	4.831	2.540	0.282	3.205
S2	1.230	0.137	73.171	2.100	0.233	42.857
S3	2.200	0.244	40.909	3.510	0.390	25.641
S4	4.150	0.461	21.687	6.990	0.777	12.876
S5	1.370	0.152	65.693	2.260	0.251	39.823
S6	2.070	0.230	43.478	3.120	0.347	28.846

After the previous investigations, the optical simulation was conducted in order to predict the device performance by determining the internal absorption of the active layer in the OPV device. As initial step in this treatment, the complex dielectric function identified by using the UV-vis measurements that imported in Reffit software [15] to fit with known theoretical models such as Drude and Lorenz) as mention early in the experimental section Figure 8 present the

real and imaginary part of dielectric for all samples and the most important part is the imaginary part as it describes the light interaction with material and it will be used in equation (1) to predict the internal absorption of the active layer.

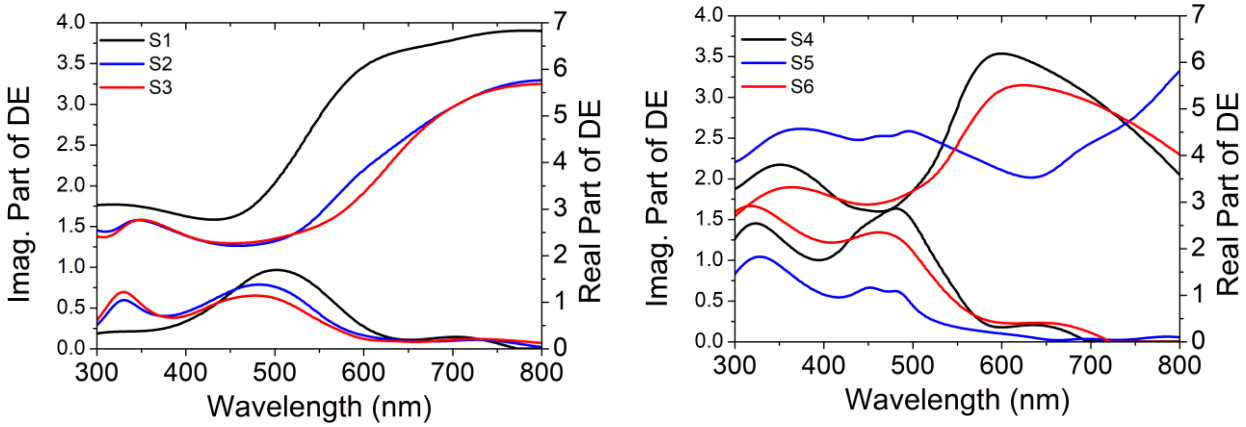

Figure 8. A complex dielectric function of P3HT: ICxA varied ration BHJ thin films (a) S1-(1:0.5) , S2-(1:0.8) and S3-(1:1) , (b) S3-(1:1.2) , S5-(1:1.5) and S6-(1:2) .

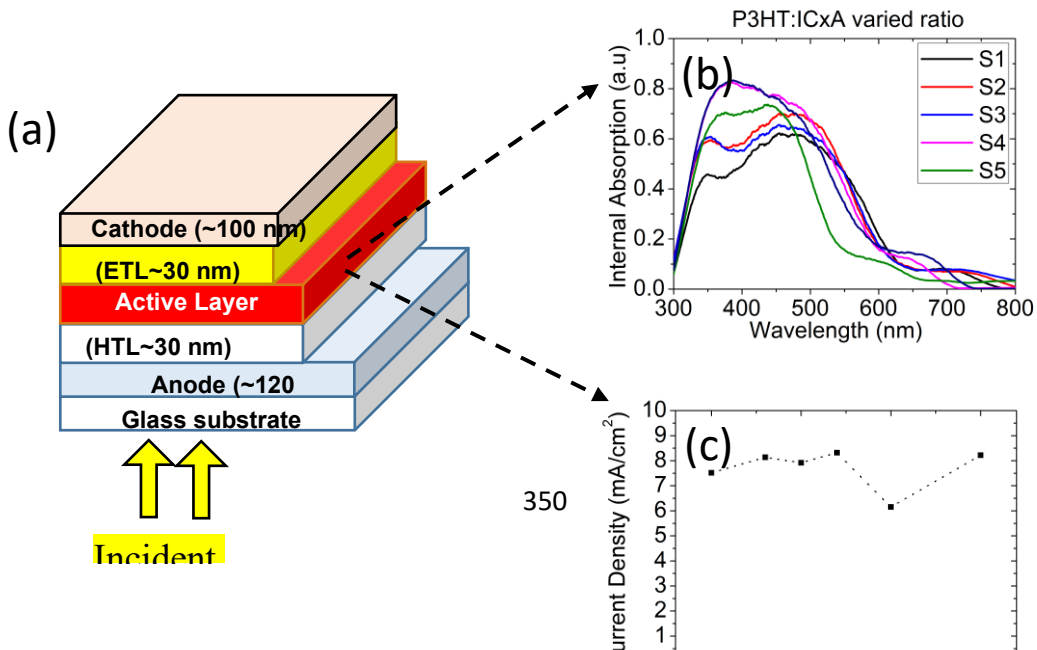

Figure 9. (a) Presents a device structure that was considered in optical modelling treatment. (b) shows the active layer internal absorption determined by the Transfer Matrix method (TMM) for four samples (S1 to S6).

Once the dielectric function is identified, the optical modelling can be conducted using MATLAB code to predict the active layer light absorption spectra, which means the distribution of the incident electric field will be determined in a multilayer system. The device structure was built in MATLAB [16] as follows (Glass/ITO/PEDOT: PSS/Active layer using varied acceptor ratio /Al), and the complex of DE of each layer was used in the simulation treatment. The optical modelling findings were presented in Figure 9, as it involves the device structure (a), (b) is the internal light absorption of the active layer (for all samples (S1 to S6). As is clear from the UV-vis measurements of all samples (S1 to S6), the fullerene light absorption increased in the wavelength range (300-400 nm), which this range refers to fullerene absorption activity, which P3HT relativity not improve in the wavelength range (400-700 nm).

To get a full idea about the device performance (theoretically), the internal absorption spectrum was convoluted with the AM1.5 spectrum to address the optimum current density (*Jsc*) of the device, assuming internal quantum efficiency equal 100% (i.e., no charge losses in the active layer). All the current density values of the samples were illustrated in Table 6. The Jsc values range from 7.518~8.319 mA/cm^{2,} and this agrees with the literature. The S4 (P3HT: ICxA (1:1.2)) exhibited the highest values, 8.319 mA/cm^2. Optical modelling findings support all the previous investigations, which confirmed that the best ratio of donor/acceptor is (1:1.2), and in comparison with a common donor/acceptor (P3HT: PCBM), is exhibited the best ratio (1:0.8) or (1:1); both of them can give a high performance for OPV devices.

Table 6. Current density values with altering acceptor ratio of P3HT: ICxA for all samples (from S1 to S6).

Sample ID:	(P3HT:ICxA)	Current Density (mA/cm^2)
S1	(1:0.5)	7.51896
S2	(1:0.8)	8.13335
S3	(1:1)	7.91848
S4	(1:1.2)	8.31907
S5	(1:1.5)	6.15046
S6	(1:2)	8.21976

4. Conclusions

In conclusion, P3HT:ICxA varied ratio thin films were prepared in order to identify the effect of changing the acceptor ratio on optical and electrical properties. The investigation of surface morphology for all samples confirmed that the RMS of roughness with in (2~4 nm). UV-vis measurements were utilized to identify the linear optical properties of the samples (S1 (P3HT: ICxA (1:0.5)), S2 (P3HT: ICxA (1:0.8)), S3(P3HT: ICxA (1:1)), S4 (P3HT: ICxA (1:1.2)), S5 (P3HT: ICxA (1:1.5)), and S6 (P3HT: ICxA (1:2)) and they confirmed that S4 (P3HT: ICxA (1:1.2)) exhibited the highest optical absorption in comparison with other samples. The P3HT: ICxA photoactive layer exhibited the direct electronic transition as the values of absorption coefficient ($\alpha > 10^4$ cm^{-1}). The electrical measurements of samples confirmed S4 (1:1.2) enhanced by a factor 2.178, 3.241, 1.895, 3.889, and 2.983 times compared with S1, S2, S3, S5, and S6, respectively at light conditions. Electrical measurements were performed for all samples by altering the sample temperature (25- 65 ^oC) at dark and light conditions, the optimum ratio (1:1.2) was 2 times higher than that of other samples. However, this type of material, P3HT: ICxA, generated a similar recorded current in both heating and cooling cycles, which emphasized the morphology of active layer remained well-ordered through both heating and cooling cycles. Optical modelling was conducted to full OPV devices and its findings confirmed all optical and electrical measurements.

References

[1] F. D'Amico, B. de Jong, M. Bartolini, et al., "Recent advances in organic dyes for application in dye-sensitized solar cells under indoor lighting conditions," *Materials*, vol. 16, no. 23, p. 7338, 2023, https://doi.org/10.3390/ma16237338.

[2] A. Mavazzan, A. C. Mendhe, P. K. Bayannavar, B. R. Sankapal, V. B. Nadoni, S. F. Madar, R. R. Kamble, K. M. M. Pasha, and B. Kodasi, "Novel 6-amino-5-cyano [2, 2′/2, 3′/2, 4′-bipyridin]-4-yl-triphenylamine dyes anchored on cadmium sulphide nanowires: Optical, electrochemical and photovoltaic applications," *Journal of Chemical Sciences*, vol. 137, no. 2, pp. 1-9, 2025, https://doi.org/10.1007/s12039-025-02357-y.

[3] L. Zhu, M. Zhang, J. Xu, et al., "Single-junction organic solar cells with over 19% efficiency enabled by a refined double-fibril network morphology," *Nature Materials*, vol. 21, no. 6, pp. 656-663, 2022, https://doi.org/10.1038/s41563-022-01244-y.

[4] Y. Wei, Z. Chen, G. Lu, et al., "Binary organic solar cells breaking 19% via manipulating the vertical component distribution," *Advanced Materials*, vol. 34, no. 33, p. 2204718, 2022, https://doi.org/10.1002/adma.202204718.

[5] A. Distler, C. J. Brabec, and H.-J. Egelhaaf, "Organic photovoltaic modules with new world record efficiencies," *Progress in Photovoltaics: Research and Applications*, vol. 29, no. 1, pp. 24-31, 2021, https://doi.org/10.1002/pip.3336.

[6] R. Basu, F. Gumpert, J. Lohbreier, et al., "Large-area organic photovoltaic modules with 14.5% certified world record efficiency," *Joule*, vol. 8, no. 4, pp. 970-978, 2024, https://doi.org/10.1016/j.joule.2024.02.016.

[7] H. S. Ryu, S. Y. Park, T. H. Lee, et al., "Recent progress in indoor organic photovoltaics," *Nanoscale*, vol. 12, no. 10, pp. 5792-5804, 2020, https://doi.org/10.1039/D0NR00816H.

[8] M. Ylikunnari, M. Välimäki, K.-L. Väisänen, et al., "Flexible OPV modules for highly efficient indoor applications," *Flexible and Printed Electronics*, vol. 5, no. 1, p. 014008, 2020, https://doi.org/10.1088/2058-8585/ab6e73.

[9] E. K. Solak and E. Irmak, "Advances in organic photovoltaic cells: a comprehensive review of materials, technologies, and performance," *RSC Advances*, vol. 13, no. 18, pp. 12244-12269, 2023, https://doi.org/10.1039/d3ra01454a.

[10] I. Persson, H. Laval, S. Chambon, G. Bonfante, K. Hirakawa, G. Wantz, B. Watts, M. A. Marcus, X. Xu, L. Ying, G. Lakhwani, M. R. Andersson, J. M. Cairney, and N. P. Holmes, "Sub-4 nm mapping of donor–acceptor organic semiconductor nanoparticle composition," *Nanoscale*, vol. 15, no. 13, pp. 6126-6142, 2023, https://doi.org/10.1039/D3NR00839H.

[11] M. T. Dang, L. Hirsch, and G. Wantz, "P3HT:PCBM, best seller in polymer photovoltaic research," *Advanced Materials*, vol. 23, no. 31, pp. 3597-3602, 2011, https://doi.org/10.1002/adma.201100792.

[12] N. A. Cooling, E. F. Barnes, F. Almyahi, et al., "A low-cost mixed fullerene acceptor blend for printed electronics," *Journal of Materials Chemistry A*, vol. 4, no. 26, pp. 10274-10281, 2016, https://doi.org/10.1039/C6TA04191D.

[13] M. Ameri, M. F. Al-Mudhaffer, F. Almyahi, et al., "Role of Stabilizing Surfactants on Capacitance, Charge, and Ion Transport in Organic Nanoparticle-Based Electronic

Devices," *ACS Applied Materials & Interfaces*, vol. 11, 2019, https://doi.org/10.1021/acsami.8b19820.

[14] B. Kadem and A. Hassan, "The Effect of Fullerene Derivatives Ratio on P3HT-based Organic Solar Cells," *Energy Procedia*, vol. 74, pp. 439-445, 2015, https://doi.org/10.1016/j.egypro.2015.07.647.

[15] A. B. Kuzmenko, "Kramers–Kronig constrained variational analysis of optical spectra," *Review of Scientific Instruments*, vol. 76, no. 8, p. 083108, 2005, https://doi.org/10.1063/1.1979470.

[16] N. C. Nicolaidis, "Optical Properties of Nanoparticulate Organic Photovoltaics and Pathways to Implementation," Thesis, 2015.

[17] R. Usmani, M. Asim, and M. Nasibullah, "Optical Modelling of Typical Organic Solar Cell using Transfer Matrix Model," *Indian Journal of Science and Technology*, vol. 15, no. 38, pp. 1965-1970, 2022, https://doi.org/10.17485/IJST/v15i38.1398.

[18] S. Jung, K.-y. Kim, Y.-i. Lee, et al., "Optical Modeling and Analysis of Organic Solar Cells with Coherent Multilayers and Incoherent Glass Substrate Using Generalized Transfer Matrix Method," *Japanese Journal of Applied Physics*, vol. 50, pp. 1-8, 2011, https://doi.org/10.1143/JJAP.50.122301.

[19] N. C. Nicolaidis, M. F. Al-Mudhaffer, J. Holdsworth, et al., "The Contribution of Fullerene Photocurrent Generation to Organic Solar Cell Performance," *The Journal of Physical Chemistry C*, vol. 123, 2019, https://doi.org/10.1021/acs.jpcc.9b01439.

[20] Z. Ma, W. Sun, S. Himmelberger, et al., "Structure–property relationships of oligothiophene–isoindigo polymers for efficient bulk-heterojunction solar cells," *Energy & Environmental Science*, vol. 7, no. 1, pp. 361-369, 2014, https://doi.org/10.1039/C3EE42989J.

[21] K. Feron, M. N. Thameel, M. F. Al-Mudhaffer, et al., "Energy level engineering in ternary organic solar cells: Evaluating exciton dissociation at organic semiconductor interfaces," *Applied Physics Letters*, vol. 110, no. 13, p. 133301, 2017, https://doi.org/10.1063/1.4979181.

[22] M. Shaban, M. Benghanem, A. Almohammedi, et al., "Optimization of the active layer P3HT: PCBM for organic solar cell," *Coatings*, vol. 11, no. 7, p. 863, 2021, https://doi.org/10.3390/coatings11070863.

[23] S. Alam, A. Anand, M. M. Islam, et al., "P3HT: PCBM polymer solar cells from a didactic perspective," *Journal of Photonics for Energy*, vol. 12, no. 3, p. 035501, 2022, https://doi.org/10.1117/1.JPE.12.035501.

تأثير نسب الفوليرين المختلطة على الخصائص البصرية والكهربائية للأغشية الرقيقة من نوع (P3HT: ICxA)ذات الوصلة الهجين المتغايرة، والنمذجة البصرية لأجهزة الخلايا الشمسية العضوية.

نور الهدى حسين علي و محمد فاضل المظفر

قسم الفيزياء, كلية التربية للعلوم الصرفة, جامعة البصرة, البصرة، العراق.

المستخلص

تم تحضير سلسلة من الأغشية الرقيقة (P3HT: ICxA) ذات الوصلة الهجين المتغايرة (BHJ) بنسب خلط مختلفة بين المانح والمستقبل، وذلك لتحديد تأثير محتوى الفوليرين على الخصائص البصرية والكهربائية للطبقة النشطة. تم أخذ ست نسب للمستقبل بعين الاعتبار هي (1:0.5، 1:0.8، 1:1، 1:1.2، 1:1.5، و 1:2). فُحصت تضاريس السطح عن طريق التقاط صور مجهر القوة الذرية (AFM)، والتي أكدت أن جميع العينات أظهرت جذر متوسط مربع خشونة (RMS) يتراوح بين (2-4 نانومتر). أظهرت القياسات البصرية لخليط (P3HT: ICxA) أن نسبة الخلط (1:1.2) حققت أعلى استجابة بصرية مقارنة بالعينات الأخرى. وبالنسبة لجميع الأغشية، حقق معامل الامتصاص قيمة (α>104 سم$^{-1}$)، مما يشير إلى حدوث انتقالات إلكترونية مباشرة داخل الطبقة النشطة. كما تم إجراء القياسات الكهربائية كدالة لدرجة حرارة العينة ضمن النطاق (25-65 درجة مئوية) في ظروف الظلام والإضاءة. ولدت الطبقة النشطة ضوئياً (P3HT: ICxA) قيماً متقاربة نسبياً للتيار في دورتي التسخين والتبريد، مما يشير إلى أن مورفولوجيا الطبقة النشطة قد وصلت للحالة المثلى وحافظت على ترتيبها الجيد طوال العملية الحرارية. وأخيراً، تم إجراء نمذجة بصرية لجهاز OPV كامل، حيث دعمت نتائجها وأكدت التوجهات التي لوحظت في كل من القياسات البصرية والكهربائية.

الكلمات المفتاحية : ICxA، الخصائص البصرية، الخصائص الكهربائية، التأثير الحراري على الخلايا الشمسية العضوية (OPVs).